CrossMark

Atomistic modeling of Mg/Nb interfaces: shear strength and interaction with lattice glide dislocations

S. K. Yadav[1,2,*] , S. Shao[2,3], Y. Chen[4], J. Wang[5], and X.-Y. Liu[2]

[1] *Department of Metallurgical and Materials Engineering, Indian Institute of Technology (IIT) Madras, Chennai 600036, India*
[2] *Materials Science and Technology Division, MST-8, Los Alamos National Laboratory, Los Alamos, NM 87545, USA*
[3] *Department of Mechanical and Industrial Engineering, Louisiana State University, Baton Rouge, LA 70803, USA*
[4] *Materials Physics and Applications Division, MPA-CINT, Los Alamos National Laboratory, Los Alamos, NM 87545, USA*
[5] *Department of Mechanical and Materials Engineering, University of Nebraska–Lincoln, Lincoln, NE 68583, USA*

ABSTRACT

Using a newly developed embedded-atom-method potential for Mg–Nb, the semi-coherent Mg/Nb interface with the Kurdjumov–Sachs orientation relationship is studied. Atomistic simulations have been carried out to understand the shear strength of the interface, as well as the interaction between lattice glide dislocations and the interface. The interface shear mechanisms are dependent on the shear loading directions, through either interface sliding between Mg and Nb atomic layers or nucleation and gliding of Shockley partial dislocations in between the first two atomic planes in Mg at the interface. The shear strength for the Mg/Nb interface is found to be generally high, in the range of 0.9–1.3 GPa depending on the shear direction. As a consequence, the extents of dislocation core spread into the interface are considerably small, especially when compared to the case of other "weak" interfaces such as the Cu/Nb interface.

Introduction

Magnesium (Mg) has a huge potential as structural materials in the aerospace and automotive industries because of its light-weight properties [1]. In its natural crystal form of hexagonal-close-packed (hcp) structure, Mg has low strength, low deformability and a high plastic anisotropy between the basal and the non-basal slip systems at room temperature. Therefore, it is strongly desirable to improve the deformability of Mg and its flow strength. Nanoscale multilayered structures with a high density of interfaces are attractive candidates to achieve high strength and high deformability. A few studies on Zr/Nb multilayered structures indicated that there is suppression of twinning boundaries in these materials [2–4]. Mg/Nb multilayered nanolaminate has been recently extensively studied. It was found that in Mg/Nb multilayers, Mg is in body-centered-cubic (bcc) phase as the thickness of Mg layers is below 5 nm [5, 6]. For thicker layer thickness, Mg in the Mg/Nb multilayers is in its hcp phase [7]. In a recent work by Pathak et al. [8], it is experimentally determined that the interfaces in the 50 nm/50 nm Mg/

Address correspondence to E-mail: satyesh@iitm.ac.in

⚛ Springer

Nb composite are {0001}Mg||{110}Nb, consistent with our internal work [9]. These experimental observations suggest that at larger thickness, semi-coherent bcc Mg region near the interface is not preferred; rather, a semi-coherent hcp Mg/bcc Nb interface is preferred. This is consistent with DFT calculations [7] that bcc Mg forms only when Mg is coherent with the Nb layer. If the layer of Mg is semi-coherent, hcp phase is preferred. The measured hardness of the Mg/Nb multilayers approaches plateau starting from 25 nm layer thickness, reaching a peak plateau of ∼ 2.7 GPa, which is greater than hardness of most other Mg and Mg alloys reported [6]. From the modeling point of view, there is generally a lack of understanding of the deformation behavior of Mg/Nb at the atomistic scale.

In this work, using a newly developed semiempirical potential for Mg/Nb alloys in the embedded-atom-method (EAM) form, we studied the semi-coherent (hcp) Mg/(bcc) Nb interface in the Kurdjumov–Sachs (KS) orientation relationship (OR) between hcp Mg and bcc Nb using atomistic simulations. The atomistic simulations are focused on the mechanical properties of such semi-coherent interface: the shear strength and associated shear mechanism of interface, and the interaction of the interface with lattice glide dislocations from bcc Nb. Since the dilute heats of mixing are positive for both Mg in bcc Nb and Nb in hcp Mg, the two elements are considered immiscible to each other. It was found in "weak" interfaces such as Cu/Nb interfaces, where both elements are immiscible, a striking feature of the interface is that when the lattice dislocations approach such interfaces, an appreciable core spread of the lattice dislocations occurs, thereby strengthening the barrier to slip transmission [10]. It is also scientifically interesting to examine the core spread of lattice dislocations in the case of Mg/Nb interfaces, to understand if "weak" interface translates to large area of core spread of dislocation at interfaces.

This paper is organized as follows. We describe the methodology of atomistic simulations in "The methodology of atomistic simulations" section. In "Shear strength and associated shear mechanism of the interface" section, the result of the shear strength and associated shear mechanism of the interface is presented. In "Interaction of lattice glide dislocations with interface" section, the interaction of lattice glide dislocations with interface is presented. Finally, a summary is given.

The methodology of atomistic simulations

Mg/Nb interatomic potential

A semiempirical potential for Mg/Nb alloy in the EAM form [11] is employed to model bulk Mg, Nb, and the interaction between Mg and Nb. The EAM potential for Mg using the force-matching method approach [12] is used, which has been widely used for modeling of the mechanical properties of hcp Mg. For Nb, the Ackland and Thetford's Finnis–Sinclair (FS) Nb potential [13] is used. The usage of the Ackland and Thetford's FS potential for Nb is due to its superior mechanical properties compared to other EAM forms [14–16]. The cross-potential between Mg and Nb is developed in this work. In the present work, we adopt the same fitting scheme as proposed earlier [17] which has been successfully applied to multiple material systems [16, 18–20]. Due to the immiscible nature in Mg–Nb systems, there is no equilibrium compound which can be used for fitting the cross-potential. The lattice constant and bulk modulus of a hypothetical B2 (CsCl) phase MgNb obtained from first-principles density functional theory (DFT) calculations were used in fitting the cross-potential. In addition, the dilute heats of mixing (Nb in Mg, and Mg in Nb) calculated from DFT were fitted. Table 1 lists the fitted properties of the newly constructed cross-potentials for the Mg–Nb systems. It can be seen that the fitting to the alloy properties is very good.

Atomistic simulations

Mg/Nb interface with KS OR has been observed experimentally before [6, 21]. For the atomistic simulations involved in the interaction of lattice dislocations with interfaces, an interface dislocation interaction model is introduced. This model is created by assembling two un-relaxed perfect crystals of hcp Mg and bcc Nb with the KS OR, as shown in Fig. 1. In KS OR, the (0001) surface of Mg is parallel to the (110) surface of Nb. At the interface, the x-axis is along $[1\bar{1}00]_{Mg}||[1\bar{1}2]_{Nb}$, and the z-axis is along $[11\bar{2}0]_{Mg}||[\bar{1}11]_{Nb}$. The interface plane is perpendicular to the y-axis. The periodic boundary conditions are applied in both the x and z directions. The dimensions in the x and z directions are chosen such that the strains imposed on the Mg and Nb crystals are negligibly small, $\epsilon_{xx}^{Mg} = -\epsilon_{xx}^{Nb} = -0.000145$ and

Table 1 Fitted properties of the newly constructed EAM cross-potentials for the Mg–Nb systems

	ΔH (Nb in Mg) (eV)	ΔH (Mg in Nb) (eV)	a_{CsCl} (Å)	B_{CsCl} (GPa)
VASP	1.24	1.16	3.35	94.6
Mg–Nb potential	1.23	1.19	3.47	94.6

ΔH is the heat of mixing. a_{CsCl} is lattice constant, and B_{CsCl} is bulk modulus of MgNb in CsCl structure
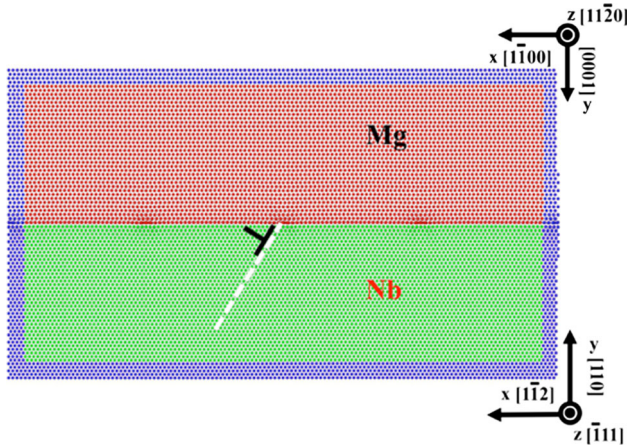

Figure 1 Simulation setup for the study of the interaction of lattice dislocations with interfaces. A periodic boundary is adopted in the z direction.

$\epsilon_{zz}^{Mg} = -\epsilon_{zz}^{Nb} = 0.00051$, while ensuring periodic boundary conditions. The bilayer model is then relaxed to reach the equilibrium, which satisfies the following conditions: (i) normal stresses σ_{yy} in the two crystals are 0, (ii) the summation of stresses in the two crystals in x direction $\sigma_{xx}^{Mg} + \sigma_{xx}^{Nb} = 0$, and (iii) the summation of stresses in the two crystals in z direction $\sigma_{zz}^{Mg} + \sigma_{zz}^{Nb} = 0$. The simulation supercell contains 16 periodic units for Mg and 11 periodic units for Nb in the x direction, and 33 periodic units for Mg and 37 periodic units for Nb in the z direction. The final dimensions of the bicrystal model are 35.56 and 10.58 nm in the x and z directions, corresponding to a supercell at equilibrium. There are 29 layer of Mg and 37 layer of Nb, with total dimension in the y direction is 19.97 nm. The quenching molecular dynamics (MD) method [22] is used to relax the bilayer model. The bilayer model has three parts in the y direction: the movable region 1 inside the simulation cell, and a semirigid region surrounding region 1 (each in Mg and Nb crystals) that is twice the potential cutoff distance in the y direction such that the two crystals can translate as rigid bodies. During

the relaxation, the atoms are relaxed until the forces are < 5 pN.

The relaxed bilayer model is used to further study the interaction of lattice glide dislocations in Nb with the interface, with a region of movable atoms in the model surrounded by a semirigid region of approximately 10 Å, as schematically shown in Fig. 1. The anisotropic elastic solution of Barnett–Lothe for an infinite bimetallic interface consisting of elastically dissimilar materials [23] is used for introduction of a lattice glide dislocation in the bilayer model. The line direction of the introduced dislocation is in the z direction in which the periodic boundary condition is applied. In x and y directions, the fixed boundaries are adopted. The fixed boundary conditions are not allowed to rigidly move or to adjust dimensions. During the tension or compression, the atoms in the fixed boundary conditions are strained accordingly. After the dislocation is introduced, the relaxation of the model containing dislocations is carried out again using the quenching MD method mentioned earlier.

For shear loading simulations of the interface, the simulation supercell has 8.89 nm along $[1\bar{1}00]_{Mg}||$ $[1\bar{1}2]_{Nb}$ in the x direction, and 5.14 nm along $[11\bar{2}0]_{Mg}||[\bar{1}11]_{Nb}$ in the z direction at the interface. The height of the supercell in the y direction (which is perpendicular to the interfaces) is 15.7 nm. The bilayer model is rectangular in shape and periodic in the x and z directions that are parallel to the interface. A gradually increasing shear strain is applied homogeneously to the bilayer model of Mg/Nb crystal. In each loading step, the stress increment is controlled to be ≤ 20 MPa [18, 24]. After each loading step, the bilayer model is relaxed through quenching MD.

For disregistry analysis, disregistry vectors $\Delta\vec{r}$ are computed as,

$$\Delta\vec{r} = \vec{r}_{ij}^{\,int} - \vec{r}_{ij}^{\,ref} \qquad (1)$$

where $\vec{r}_{ij}^{\,ref}$ is the relative position between the ith atom and the jth atom that form a pair in the reference configuration and $\vec{r}_{ij}^{\,int}$ is the relative position

between the same pair of atoms [10, 18, 25]. For in-plane disregistry analysis, the disregistry vectors are projected into the plane of choice.

Shear strength and associated shear mechanism of the interface

A summary of the interface misfit dislocations at KS interface

We have analyzed interface dislocation networks at Mg/Nb interfaces by using Frank–Bilby analysis with atomistic simulations as input [21, 26]. Here, we briefly summarize such interface dislocation network at the KS interface and detailed information is referred to Ref. [21]. At KS interface between Mg and Nb layers at the interface, three sets of partial dislocations nucleate around nodes during interface relaxation and among them, two close partial dislocations react to form one set of full dislocations and therefore we obtain 4 sets of dislocations ($\mathbf{b_1}$–$\mathbf{b_4}$) as shown in Fig. 2. The disregistry analysis in Fig. 2a is performed with respect to un-relaxed structure, where the Burgers vector content within a periodic length of the two-dimensional boundary unit cell (BUC) is zero, and thus the disregistry analysis could be employed to illustrate the overall feature of dislocation network, such as the line sense, spacing and location of dislocations. As shown in Fig. 2, interface dislocations $\mathbf{b_1}$–$\mathbf{b_3}$ are partial dislocations and have dislocation lines along the z-axis, with an average spacing of 8.89 nm; interface dislocation $\mathbf{b_4}$ has the dislocation line 56.8° inclined with respect to the x-axis, Burgers vector $-b_R^{II}$, and an average spacing of 1.40 nm. It is worth mentioning that the coherent structures in between dislocations can be stacked into either normal fcc structures (FCC in Fig. 2a) or low-energy stacking faulted structures (SF in Fig. 2a). The detailed energetics is referred to [21]. In summary, KS interface is composed of four sets of interface dislocations—three sets of partial dislocations and one set of full dislocations that forms from the reaction of two close partial dislocations.

Shear loading simulations

In Fig. 3, the critical stresses for the shear sliding at the Mg/Nb interface in KS OR are shown as a function of different shear loading directions. The applied
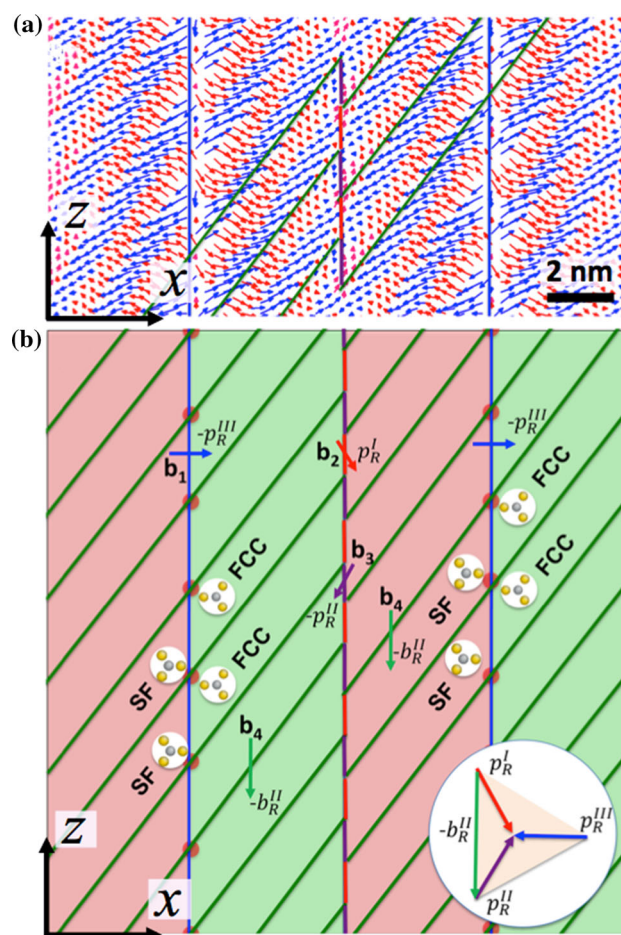

Figure 2 Interface dislocations of the KS interface **a** disregistry plot; **b** schematic of interface dislocation network. FCC represents coherent interface with fcc stacking (…A(Mg)B(Mg)/C(Nb)…) and SF represents coherent interface with low-energy stacking (…A(Mg)B(Mg)/A(Nb)…).

shear strain is a combination of ε_{yx} and ε_{yz}, parallel to the interface and along the x- or z-axis. The critical stress is the effective shear stress, $\sigma_c = \sqrt{\left(\sigma_{yx}^2 + \sigma_{yz}^2 \right)}$ at the onset of unstable shear transition point in the stress–strain curve obtained during shear loading simulations. In the process of determining the effective shear stress, the temporal plastic transition is ignored if this transition is followed by another shear transition of higher effective shear stress. In such cases, the latter value is taken as the critical stress. The applied shear loading is along six different directions. In the Mg lattice notation, these are: $[11\bar{2}0]$ (set 1, z-axis), $[10\bar{1}0]$ (set 2, 60° from x-axis), $[2\bar{1}\bar{1}0]$ (set 3, 30° from x-axis), $[1\bar{1}00]$ (set 4, x-axis), $[1\bar{2}10]$ (set 5, − 30° from x-axis), and $[0\bar{1}10]$ (set 6, − 60° from x-
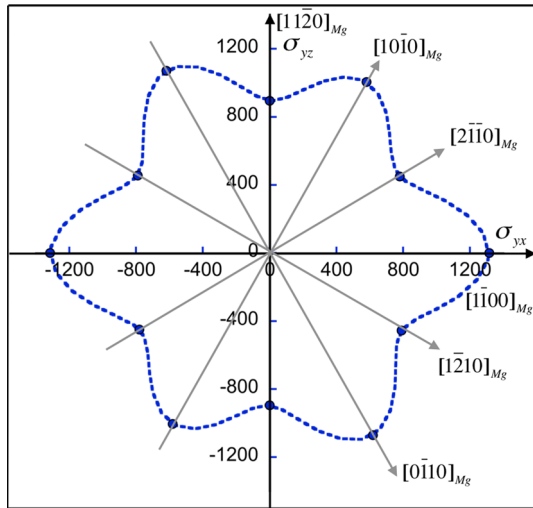
Figure 3 Critical stresses for the shear sliding at the Mg/Nb interface in KS OR, as a function of different shear loading directions. The stresses are in MPa unit.
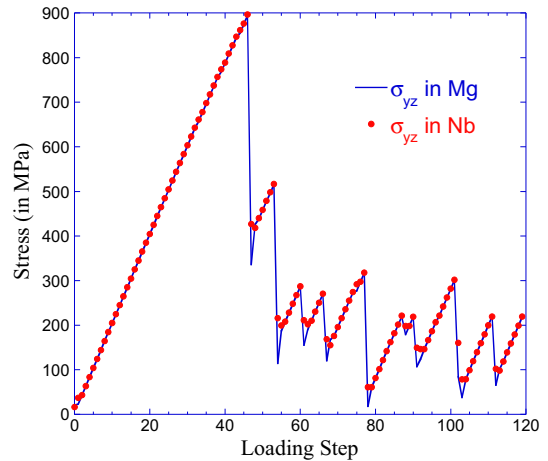

Figure 4 Stress σ_{yz} as a function of loading steps in the Mg and Nb parts in the bilayer model of Mg/Nb crystal during shear loading in the z-axis $[11\bar{2}0]_{Mg}||[\bar{1}11]_{Nb}$.

axis) (see also labels in Fig. 3). The critical shear stress values are listed in Table 2. There is a strong anisotropy of the critical shear stress values for loading in different directions. The maximum critical shear stress at the KS interface is along the x-axis, 1315 MPa, and the minimum critical shear stress is along the z-axis, 895 MPa. The interface shear strength for Mg/Nb interface in the range of 0.9–1.3 GPa is generally higher than in the Cu/Nb interfaces [24]. Considering that the shear modulus of Cu (81.8 GPa) is 4.4 times of Mg (18.4 GPa), such interface shear strength values imply a high resistance at the interface. In the following, we analyze the interface shearing mechanisms.

In Fig. 4, the stress–strain relationship during shear loading in the z-axis, $[11\bar{2}0]_{Mg}||[\bar{1}11]_{Nb}$ is shown: stress σ_{yz} as a function of loading steps in the Mg and Nb parts in the bilayer model of Mg/Nb crystal. The loading direction is a close-packed direction in the hcp Mg. Immediately after reaching the critical shear stress, there is a large drop of stress level followed by smaller stepwise changes in the stress–stain curve. In Fig. 5a, the interface atomic configuration between Mg and Nb layers at the interface colored by the magnitude of atomic displacements during

relaxations right after the critical stress point is shown. A marked transition of colored regions suggests slip behavior at the interface. In Fig. 5b, the corresponding in-plane disregistry vectors are plotted. The reference state for the disregistry analysis is the un-relaxed interface structure. The disregistry analysis clearly shows the slip along one of the misfit dislocation lines along the z direction which is marked as a dashed line, with Burgers vector $[11\bar{2}0]a_{Mg}/3$. A serrated feature also appears in Fig. 5a–b, which is presumably influenced by the additional misfit dislocation sets at the interface.

The stress–strain relationship exhibits a substantial difference if the shear loading is applied in the orthogonal direction. In the case of shear loading along the x-axis, or $[1\bar{1}00]_{Mg}||[1\bar{1}2]_{Nb}$, the stress–strain curve, as shown in Fig. 6a, has an initial onset of unstable shear transition followed by almost linear elastic behavior up to 1315 MPa, at which the second shear transition occurs. Disregistry analysis shows that at the initial onset of shear transition, the shear displacements are close to the Shockley partials between the 1st Mg layer and the 2nd Mg layer at the interface, thus changing the ABABAB stacking sequence into CBABAB, a local fcc ordering of Mg at the interface (Fig. 6b). As the shear loading continues,
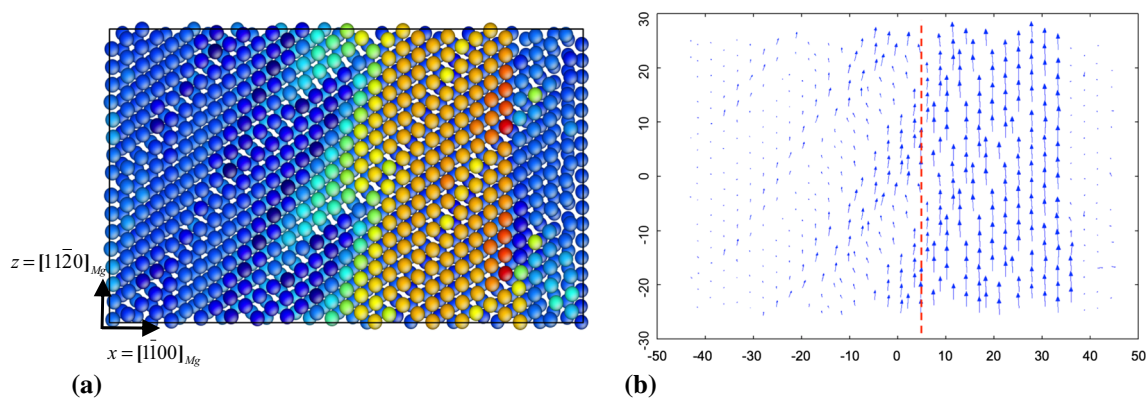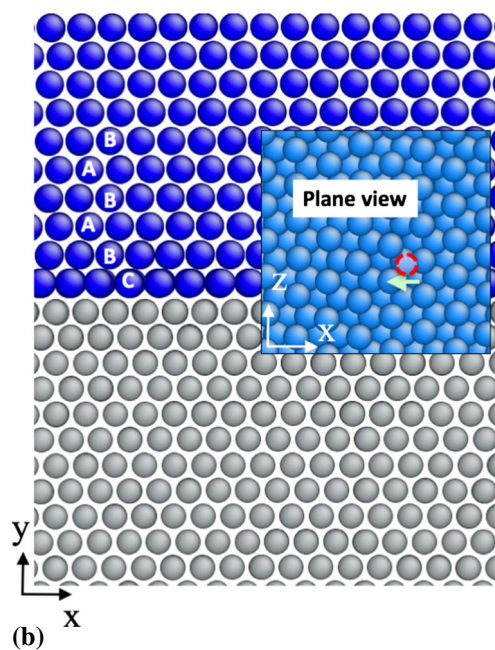
Table 2 Critical stresses for the shear sliding at the Mg/Nb interface in KS OR

Loading direction	$[11\bar{2}0]$	$[10\bar{1}0]$	$[2\bar{1}\bar{1}0]$	$[1\bar{1}00]$	$[1\bar{2}10]$	$[0\bar{1}10]$
Degrees from x-axis (°)	90	60	30	0	− 30	− 60
Critical stress (MPa)	895	1161	900	1315	912	1237

Figure 5 a For shear loading along $[11\bar{2}0]$, the z-axis, the interface atomic configuration between Mg and Nb layers at the KS Mg/Nb interface colored by the magnitude of atomic displacement during relaxations right after the critical shear stress is reached. The Mg atoms are on top. This figure is generated using Atomeye [27]. **b** The corresponding in-plane disregistry vectors.
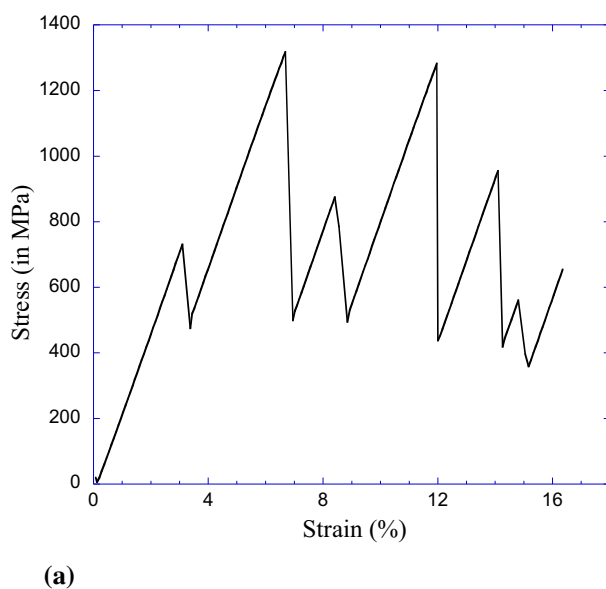
Figure 6 a Stress σ_{yx} as a function of applied shear strain during shear loading along the x-axis, $[1\bar{1}00]_{Mg}\|[112]_{Nb}$. **b** The interface atomic configuration at the initial onset of shear transition in (**a**). The stacking sequence of Mg atoms near the interface is shown. In the inset, viewing at the interface from the Mg side. The shearing direction is shown as an arrow. The blue atoms are Mg, and gray atoms are Nb.

the shear displacement progresses toward the same direction, going through an unstable stacking fault barrier (Fig. 6b, inset). Along this direction, in order for a continued Shockley partial displacement to occur, a much higher effective shear stress is required than the initial one.

For shear loading along the $[2\bar{1}\bar{1}0]_{Mg}$, or 30° from the x-axis, the interface shearing mechanism is similar to that in the case of shear loading along the x-axis. The shear displacement of Shockley partials between the 1st Mg layer and the 2nd Mg layer at the interface plays a major role in the plastic yielding during the loading process. Since the loading direction is 30° away from the x-axis, the shear displacements are able to follow the directions of the regular Shockley partials in the Mg (0001) plane at the interface, without moving toward the unstable stacking fault barrier direction. Therefore, the critical shear stress in this case is substantially reduced compared to the case of shear loading along the x-axis. The

angular effect has been reported in earlier work of fcc/bcc interface shear strength studies [18]. The effect of Schmid factor has to be taken into account as well in this case. The same scenario also happens for shear loading along the [$1\bar{2}10$] ($-30°$ from the x-axis) direction. At last, for both shear loadings along the [$10\bar{1}0$] ($60°$ from x-axis) and [$0\bar{1}10$] ($-60°$ from the x-axis), the shearing mechanisms at the interface are similar to those in the case of shear loading along the z-axis, [$11\bar{2}0$]$_{Mg}$ || [$\bar{1}11$]$_{Nb}$. Here, again, a Schmid factor has to be applied, so a higher critical shear stress is expected in both cases than in the shear loading along the z-axis.

From the analysis above, it is suggested that the deformation mechanisms are anisotropic, involving either slip along the interface dislocations between the Mg and Nb layers at the interface, or the shear displacements of Shockley partials between the 1st and 2nd Mg layers at the interface. As a result, the critical stress values are also strongly anisotropic.

Interaction of lattice glide dislocations with interface

Slip systems in (hcp) Mg/(bcc) Nb

The active slip systems for a layered (hcp) Mg/(bcc) Nb geometry subjected to either compressive stress normal to the interface plane or tensile stress parallel to the interface plane are considered. In these two situations, there is no resolved shear stress on the glide planes that make up the interface plane. So, only slip planes that are non-parallel to interface are considered. Common slip systems in Mg include basal, prismatic {$1\bar{1}00$}, pyramidal I {$1\bar{1}01$}, pyramidal II {$11\bar{2}2$}, tensile twinning planes {$1\bar{1}02$} and {$11\bar{2}1$}, and compressive twinning planes {$1\bar{1}01$} and {$11\bar{2}2$} [28]. In Nb, there are six {110} slip planes. The slip planes in Mg and Nb that are non-parallel to the interface plane have traces of intersections at the interface plane. This is shown in Fig. 7a for the KS interface. These slip planes have finite resolved shear stress for uniaxial loading normal or parallel to the interface. For all the active slip planes in Mg and Nb, there is only one common trace of intersection at the interface, i.e., [$11\bar{2}0$] for Mg and [$\bar{1}11$] for Nb. Among those slip planes that have common trace of intersection, the pyramidal I slip plane ($1\bar{1}01$) in Mg is

nearly parallel to the ($01\bar{1}$) slip plane in Nb, as shown in Fig. 7b. It is also noted that the lengths of Burgers vectors of dislocations in Mg (3.206 Å) and Nb (2.859 Å) are different. Such discontinuity in the Mg/Nb layered composites makes dislocation transmission particularly difficult. In this work, we choose the lattice glide dislocations on the Nb side to be in slip plane ($01\bar{1}$), with dislocation line directions along [$\bar{1}11$], or the z-axis of the bilayer model.

Results

We study eight cases as listed in Table 3, $1/2[111](01\bar{1})$ and $1/2[\bar{1}\bar{1}1](01\bar{1})$ mixed dislocations, and $1/2[\bar{1}11](01\bar{1})$ and $1/2[1\bar{1}1](01\bar{1})$ screw dislocations, intersecting with the interface at the primary dislocation lines (PDL) of the misfit dislocations and at the middle position in between two PDLs (Mid). A schematic describing the PDL and Mid positions where lattice glide dislocations intersect to the interface is shown in Fig. 8. Table 3 also summarizes the direction of forces exerted on the lattice glide dislocations introduced in Nb. Except for the screw dislocation that intersects at the PDL position, all other lattice glide dislocations experience attractive forces and spontaneously enter the interface upon atomistic relaxation. The force on the lattice glide dislocation is due to the Koehler force and possible tendency for interface shear when the dislocations approach toward the interface. The Koehler force is always attractive for lattice glide dislocations in Nb because of the higher effective shear modulus in Nb than in Mg. The repulsive force could be from the interaction of interface misfit dislocations with the lattice glide dislocations. If the lattice glide dislocation does not enter the interface, an external strain is applied on the bilayer model so that the lattice glide dislocation can move to the interface along the glide plane.

Mixed character lattice glide dislocations

Mixed character dislocations $1/2[111](01\bar{1})$ and $1/2[\bar{1}\bar{1}1](01\bar{1})$ are introduced in the Nb crystal of the bilayer model at a distance of 1.5 nm from the interface. They intersect at two distinct locations at the interface, PDL and Mid. As the supercell is relaxed, the dislocations spontaneously move toward interface, by gliding on ($01\bar{1}$) plane.
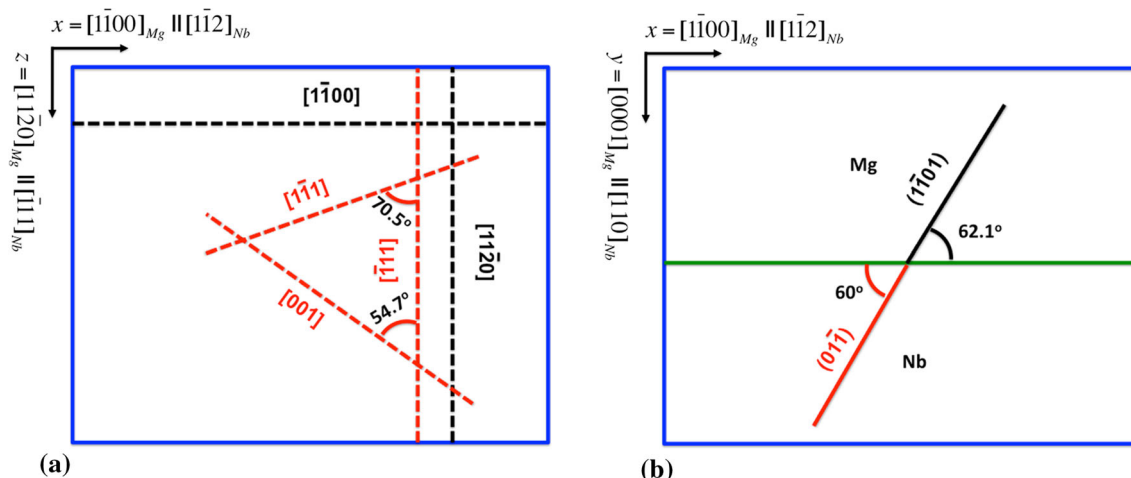
(a)

(b)

Figure 7 **a** Traces of intersections of slip and twinning planes in Mg and {110} Nb slip planes with the KS interface. Two black dashed lines, parallel to Mg $[1\bar{1}00]$ and $[11\bar{2}0]$ lines, represent intersections of the interface plane with the Mg slip and twinning planes. Three red dashed lines represent intersections of the interface plane with {110} Nb slip planes. **b** $(01\bar{1})$ and $(1\bar{1}01)$ planes are almost parallel to each other.

Table 3 Direction of forces exerted by the KS Mg/Nb interface on lattice dislocations approaching the interface from Nb

Lattice dislocation types	PDL	Mid
Mixed $[111](01\bar{1})$	Attracted	Attracted
Mixed $[\bar{1}\bar{1}\bar{1}](01\bar{1})$	Attracted	Attracted
Screw $[\bar{1}11](01\bar{1})$	Attracted after loading	Attracted
Screw $[1\bar{1}\bar{1}](01\bar{1})$	Repelled	Attracted

Lattice dislocations intercept at the PDL and Mid positions at the interface
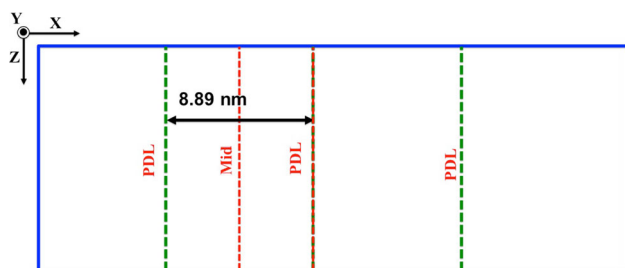

Figure 8 Schematic of supercell showing locations of primary misfit dislocations (green dashed lines) in the KS Mg/Nb interface. Lattice glide dislocations can intersect with the interface at one of the primary dislocation lines (PDL) of the misfit dislocations or at positions in between two PDLs (Mid). Trace of lattice glide dislocation intersecting at the interface is shown by red dashed line.

The disregistry analysis of lattice glide dislocations in the interface plane as well as in the glide plane is carried out. The fully relaxed Mg/Nb bilayer model before the introduction of lattice dislocations is taken as the reference structure. Nb atom layer near the interface is plotted in the disregistry plot in the interface plane. Figure 9 shows the disregistry plots of lattice glide dislocations (a) in the interface plane and (b) in the glide plane when the mixed dislocation $1/2[111](01\bar{1})$ intercepts at the PDL position. Mixed dislocation $1/2[\bar{1}\bar{1}\bar{1}](01\bar{1})$, which has negative line sense direction compared to $1/2[111](01\bar{1})$, has similar behavior. The cores of lattice glide dislocations spread into intricate patterns within the interface. This feature is ascribed to spatial non-uniformity of interfacial shear resistance. The disregistry plot in the glide plane suggests that the glide dislocation did not move into Mg. Figure 10 shows the disregistry plots of lattice glide dislocations (a) in the interface planes and (b) in the glide plane when mixed dislocation $1/2[111](01\bar{1})$ intercepts at the Mid position. The cores of lattice glide dislocations spread much less into interface compared to the case where the mixed dislocations intersecting at PDL position. Although the dislocation cores do not have much spread in the interface plane, there is possibility that the dislocation core could spread out of the interface plane. Figure 10b indicates that the glide dislocation core has spread into Mg pyramidal I slip plane $(1\bar{1}01)$.

To quantify the extent of core spread of dislocations within the interfaces, the sheared area S is computed in the form [22]:
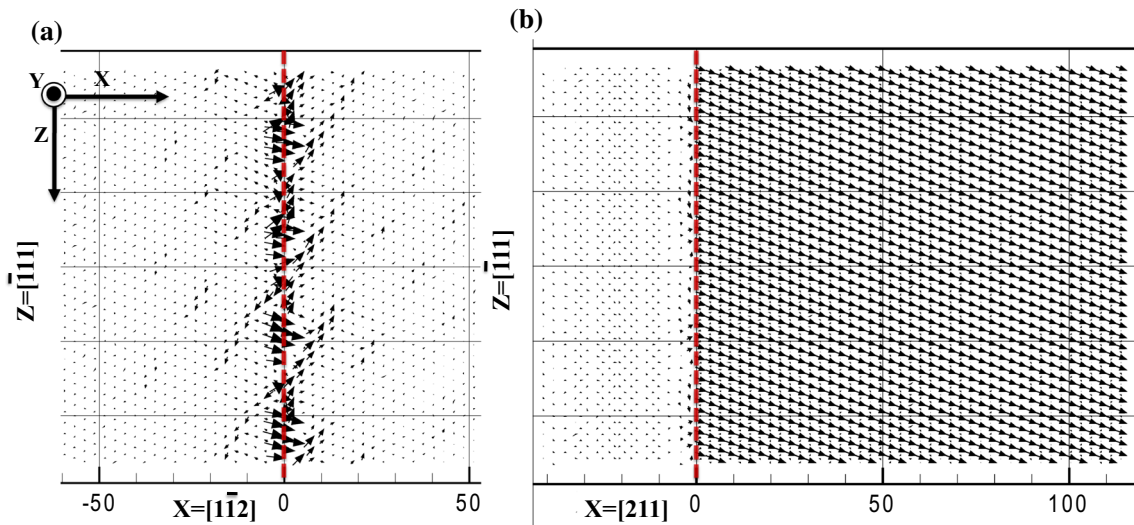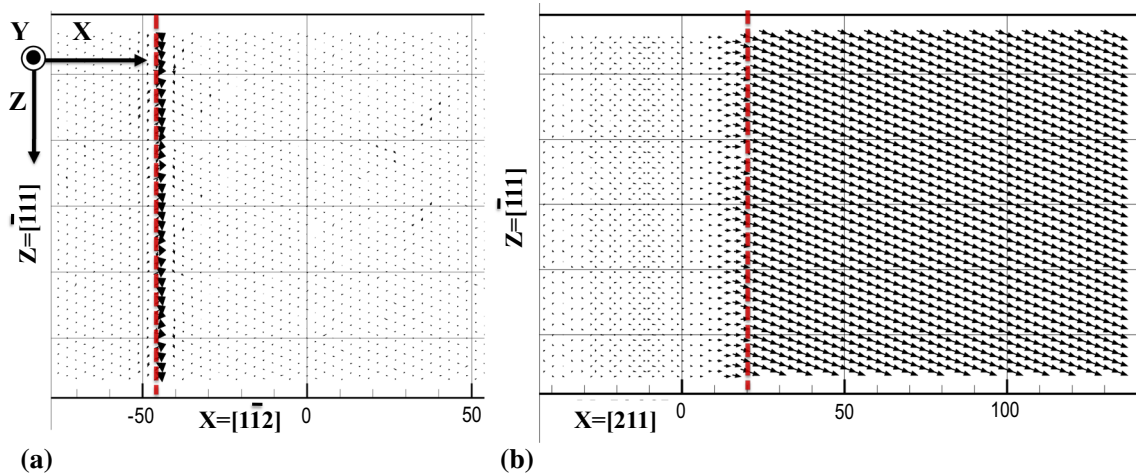
Figure 9 Vector field plot of disregistry **a** in the interface plane and **b** in the slip plane, for the case when the mixed lattice dislocation intercepts at PDL. Red dotted line indicates the intercept line of the lattice glide dislocation. Magnification factor of vector plots for (**a**) and (**b**) is 3 and 1, respectively.

Figure 10 Vector field plot of disregistry **a** in the interface plane and **b** in the slip plane, for the case when the mixed lattice dislocation intercepts at Mid. Red dotted line indicates the intercept line of the lattice glide dislocation. Magnification factor of vector plots for (**a**) and (**b**) is 3 and 1, respectively.

$$ S = \frac{1}{L} \int_{-L/2}^{L/2} \int_{-\infty}^{\infty} \left| d_{(x,z)} \right| \mathrm{d}x\mathrm{d}z \qquad (2) $$

The length of the dislocation line is denoted by L along the periodic direction z in the model and the local shear displacement at position (x, z) is $d_{(x, z)}$ in the interface plane, as determined from the disregistry analysis. Table 4 lists the sheared area S values for each case.

To understand the core spread out of the interface plane, the disregistry vectors in the glide plane are analyzed further. For mixed dislocations considered in this study, the mixed component consists of mostly edge component (2.7 Å), and the screw component is relatively small (0.95 Å). In order to compare the extent of core spread into Mg when the mixed dislocation intersects at PDL and Mid positions, we calculate the disregistry vectors in the glide plane. These disregistry vectors are then projected along the edge dislocation direction (the edge component). The values are color mapped to the atoms in the bilayer model, as shown in Fig. 11. In the case when the mixed dislocation intersects at Mid position, the

Table 4 Sheared area to quantify the core spread of dislocations within the interfaces, in 10^{-2} nm^2 unit

Lattice dislocation types	S_{PDL} (Å^2)	S_{Mid} (Å^2)	$S_{Cu/Nb}$ (Å^2) [22]
Mixed $[111](01\bar{1})$	27.4	18.0 (25.8)	125
Mixed $[\bar{1}1\bar{1}](01\bar{1})$	29.3	19.5 (26.3)	–
Screw $[\bar{1}11](01\bar{1})$	20.3	46.7	–
Screw $[1\bar{1}\bar{1}](01\bar{1})$	–	45.4	–

Lattice dislocations intercept at the PDL and Mid positions at the interface. The values in bracket are the core spreading of dislocations within the pyramidal I slip plane $(1\bar{1}01)$ in Mg
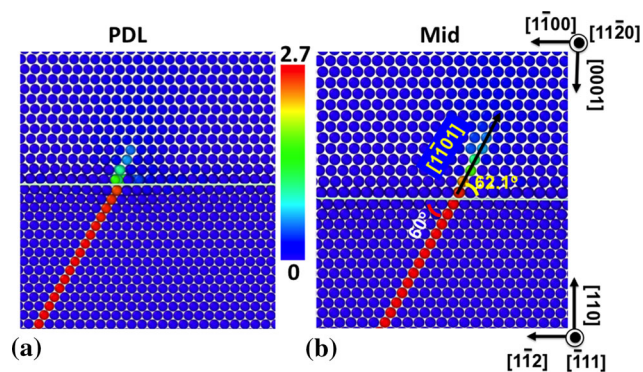

Figure 11 Absolute value of the edge component of disregistry vectors calculated along the glide plane of mixed dislocations in Nb. Mixed dislocations intersect at **a** PDL position and **b** Mid position.

dislocation core spreads into Mg for more than two atomic layers, in contrast to the case when the mixed dislocation intersects at PDL position where there is little core spread into Mg. The spread of dislocation core into Mg occurs on the pyramidal I slip plane $(1\bar{1}01)$ in Mg. This core spread provides possibility to nucleate pyramidal I type dislocation in Mg and thus facilitate dislocation slip transmission across interface. This can be investigated further in future study.

Screw character lattice glide dislocations

Screw dislocations $1/2[\bar{1}11](01\bar{1})$ and $1/2[1\bar{1}\bar{1}](01\bar{1})$ are introduced in the Nb crystal of the bilayer model, also at a distance of 1.5 nm from the interface. They intersect the interface at PDL and MID positions as well. As the supercell is relaxed, the screw dislocations experience attractive or repulsive force, depending on the location of intersection. If the screw dislocation intersects at PDL position, it does not spontaneously move toward the interface. However, if it intersects at Mid position, it spontaneously moves toward interface by gliding on $(01\bar{1})$ plane. Screw dislocation $1/2[\bar{1}11](01\bar{1})$ moves toward the

interface after applied shear stress in excess of 0.9 GPa, while screw dislocation $1/2[1\bar{1}\bar{1}](01\bar{1})$ does not move toward the interface even at applied shear stress of 4 GPa.

Figure 12 shows the extent of core spread in the interface plane. The extent of core spread in the interface plane is much larger when the screw dislocation intersects at the Mid position compared to when it intersects at the PDL position. The sheared area S calculated for screw dislocation intersecting at Mid position, as listed in Table 4, is more than twice larger the S value for screw dislocation intersecting at PDL position. No core spread into Mg was observed in either case.

So far, we have shown that the screw dislocations have larger core spread when the dislocations are away from the primary interface misfit dislocation lines at the interface. For the mixed dislocations, the opposite is true. In addition, when the dislocations are away from the primary interface misfit dislocation lines at the interface, the core of dislocations spreads into the Mg pyramidal I plane. In general, the core spreads of the screw dislocations are more appreciable than the mixed dislocations in the Mg/Nb interfaces. Such trend is also observed in other "weak" interfaces such as Cu/Nb interfaces [24]. However, for mixed dislocations, the dislocation core spreading into the interface plane is considered to be rather small, only about 23% compared to the case of Cu/Nb KS interface, as shown in Table 4 [22]. We expect the screw dislocations, similar trend will also hold. Therefore, by examining the core spread of lattice dislocations in the case of Mg/Nb interface, it is suggested that the trend of large core spread of the lattice dislocations is not observed. This correlates well with the result of interface shear strength calculations for the Mg/Nb interface. Generally, an interface with stronger interface shear strength should make it less easy for the interface to be sheared by impinging lattice glide dislocations.
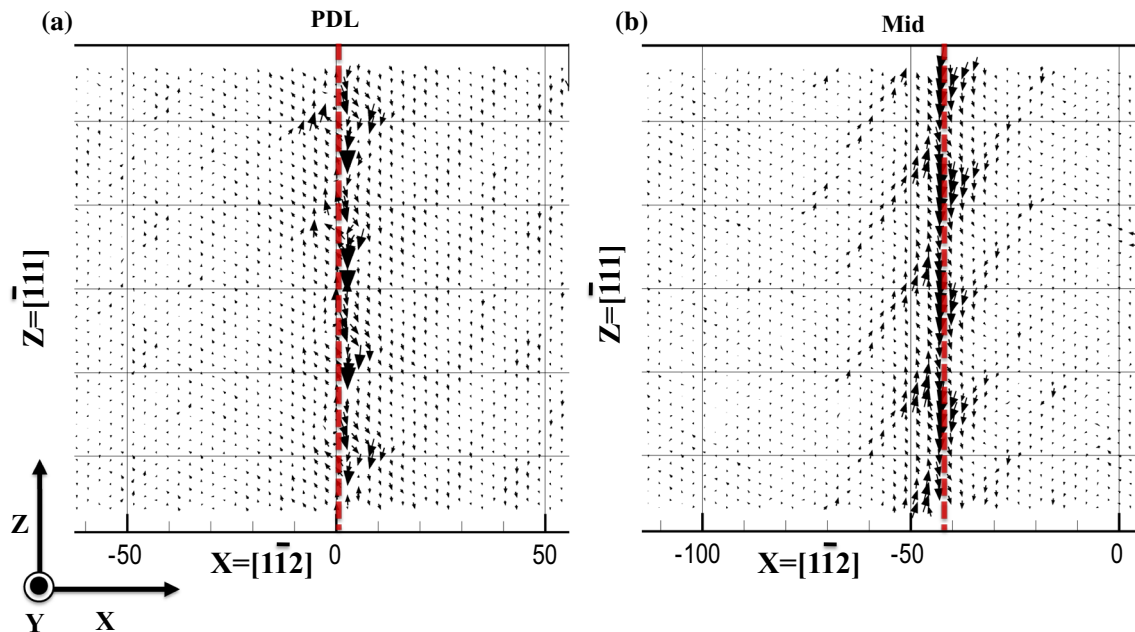
Figure 12 Vector field plot of disregistry in the interface plane for the case when the screw lattice dislocation intercepts at **a** PDL, and **b** Mid positions. Red dotted line indicates the intercept line of the lattice glide dislocation. Magnification factor of vector plots is 3.

Summary

Atomistic simulations using newly developed EAM interatomic potential for Mg–Nb have been carried out to study (hcp) Mg/(bcc) Nb semi-coherent interface with Kurdjumov–Sachs orientation relationship. The simulations are focused on the shear strength and associated shear mechanism of the interface, and the interaction between the lattice glide dislocations and the interface. The major findings are summarized as follows: (1) The interface shear deformation is strongly anisotropic, involving either slip along the interface dislocations between the Mg and Nb layers at the interface, or the shear displacements of Shockley partials between the 1st and 2nd Mg layers at the interface. The shear strength for the Mg/Nb interface is found to be generally high, in the range of 0.9–1.3 GPa depending on the shear direction. (2) The extent of the core spread of dislocations into the Mg/Nb interface is considerably small, especially when compared to the Cu/Nb case. It is suggested that the trend of large core spread of lattice dislocations at the interface formed by immiscible elements such as Cu/Nb interface is not observed in Mg/Nb. This correlates well with the result of interface shear strength calculations for the Mg/Nb interface. (3) When the mixed character lattice dislocation approaches the interface, there is core spread out of the interface plane into Mg, corresponding to the pyramidal I slip plane in Mg.

Acknowledgements

References

[1] Pollock TM (2010) Weight loss with magnesium alloys. Science 328(5981):986–987. doi:10.1126/science.1182848

[2] Ardeljan M, Beyerlein IJ, Knezevic M (2014) A dislocation density based crystal plasticity finite element model: application to a two-phase polycrystalline HCP/BCC composites. J Mech Phys Solids 66:16–31. doi:10.1016/j.jmps.2014.01.006

[3] Ardeljan M, Knezevic M, Nizolek T, Beyerlein IJ, Mara NA, Pollock TM (2015) A study of microstructure-driven strain localizations in two-phase polycrystalline HCP/BCC composites using a multi-scale model. Int J Plast 74:35–57. doi:10.1016/j.ijplas.2015.06.003

[4] Knezevic M, Nizolek T, Ardeljan M, Beyerlein IJ, Mara NA, Pollock TM (2014) Texture evolution in two-phase Zr/Nb

lamellar composites during accumulative roll bonding. Int J Plast 57:16–28. doi:10.1016/j.ijplas.2014.01.008

[5] Junkaew A, Ham B, Zhang X, Talapatra A, Arróyave R (2013) Stabilization of bcc Mg in thin films at ambient pressure: experimental evidence and ab initio calculations. Mater Res Lett 1(3):161–167

[6] Ham B, Zhang X (2011) High strength Mg/Nb nanolayer composites. Mater Sci Eng A Struct 528(4–5):2028–2033. doi:10.1016/j.msea.2010.10.101

[7] Kumar A, Beyerlein IJ, Wang J (2014) First-principles study of the structure of Mg/Nb multilayers. Appl Phys Lett 105(7):071602

[8] Pathak S, Velisavljevic N, Baldwin JK, Jain M, Zheng S, Mara NA, Beyerlein IJ (2017) Strong, ductile, and thermally stable bcc-Mg Nanolaminates. Sci Rep Uk 7(1):8264. doi:10.1038/s41598-017-08302-5

[9] Chen Y Unpublished

[10] Wang J, Hoagland RG, Hirth JP, Misra A (2008) Atomistic modeling of the interaction of glide dislocations with "weak" interfaces. Acta Mater 56(19):5685–5693. doi:10.1016/j.actamat.2008.07.041

[11] Daw MS, Baskes MI (1984) Embedded-atom method—derivation and application to impurities, surfaces, and other defects in metals. Phys Rev B 29(12):6443–6453. doi:10.1103/Physrevb.29.6443

[12] Liu XY, Adams JB, Ercolessi F, Moriarty JA (1996) EAM potential for magnesium from quantum mechanical forces. Model Simul Mater Sci 4(3):293–303

[13] Ackland GJ, Thetford R (1987) An improved N-body semiempirical model for body-centered cubic transition-metals. Philos Mag A 56(1):15–30

[14] Zhang RF, Wang J, Beyerlein IJ, Germann TC (2011) Twinning in bcc metals under shock loading: a challenge to empirical potentials. Philos Mag Lett 91(12):731–740. doi:10.1080/09500839.2011.615348

[15] Zhang RF, Germann TC, Liu XY, Wang J, Beyerlein IJ (2014) Layer size effect on the shock compression behavior of fcc–bcc nanolaminates. Acta Mater 79:74–83. doi:10.1016/j.actamat.2014.07.016

[16] Zhang L, Martinez E, Caro A, Liu X-Y, Demkowicz MJ (2013) Liquid-phase thermodynamics and structures in the Cu–Nb binary system. Model Simul Mater Sci 21(2):025005

[17] Demkowicz MJ, Hoagland RG (2009) Simulations of Collision Cascades in Cu–Nb Layered Composites Using an Eam Interatomic Potential. Int J Appl Mech 1(3):421–442

[18] Liu XY, Hoagland RG, Wang J, Germann TC, Misra A (2010) The influence of dilute heats of mixing on the atomic structures, defect energetics and mechanical properties of fcc–bcc interfaces. Acta Mater 58(13):4549–4557. doi:10.1016/j.actamat.2010.05.008

[19] Liu XY, Hoagland RG, Demkowicz MJ, Nastasi M, Misra A (2012) The influence of lattice misfit on the atomic structures and defect energetics of face centered cubic-body centered cubic interfaces. J Eng Mater T Asme 134(2):021012

[20] Wei QM, Liu XY, Misra A (2011) Observation of continuous and reversible bcc-fcc phase transformation in Ag/V multilayers. Appl Phys Lett 98(11):111907

[21] Chen Y, Shao S, Liu XY, Yadav SK, Li N, Mara N, Wang J (2017) Misfit dislocation patterns of Mg–Nb interfaces. Acta Mater 126:552–563. doi:10.1016/j.actamat.2016.12.041

[22] Wang J, Hoagland R, Liu X, Misra A (2011) The influence of interface shear strength on the glide dislocation–interface interactions. Acta Mater 59(8):3164–3173

[23] Barnett DM, Lothe J (1974) An image force theorem for dislocations in anisotropic bicrystals. J Phys F Met Phys 4(10):1618

[24] Wang J, Hoagland R, Hirth J, Misra A (2008) Atomistic simulations of the shear strength and sliding mechanisms of copper–niobium interfaces. Acta Mater 56(13):3109–3119

[25] Pilania G, Thijsse BJ, Hoagland RG, Lazic I, Valone SM, Liu XY (2014) Revisiting the Al/Al$_2$O$_3$ interface: coherent interfaces and misfit accommodation. Sci Rep Uk 4:4485

[26] Hirth J, Pond R, Hoagland R, Liu X-Y, Wang J (2013) Interface defects, reference spaces and the Frank-Bilby equation. Prog Mater Sci 58(5):749–823

[27] Li J (2003) AtomEye: an efficient atomistic configuration viewer. Model Simul Mater Sci 11(2):173–177

[28] Fan HD, El-Awady JA (2015) Molecular dynamics simulations of orientation effects during tension, compression, and bending deformations of magnesium nanocrystals. J Appl Mech T Asme 82(10):101006